Statistical Mechanics Analysis of LDPC Coding in MIMO Gaussian Channels

Roberto C. Alamino and David Saad

Neural Computing Research Group, Aston University, Birmingham B4 7ET, UK

Abstract. Using analytical methods of statistical mechanics, we analyse the typical behaviour of a multiple-input multiple-output (MIMO) Gaussian channel with binary inputs under LDPC network coding and *joint decoding*. The saddle point equations for the replica symmetric solution are found in particular realizations of this channel, including a small and large number of transmitters and receivers. In particular, we examine the cases of a single transmitter, a single receiver and the symmetric and asymmetric interference channels. Both dynamical and thermodynamical transitions from the ferromagnetic solution of perfect decoding to a non-ferromagnetic solution are identified for the cases considered, marking the practical and theoretical limits of the system under the current coding scheme. Numerical results are provided, showing the typical level of improvement/deterioration achieved with respect to the single transmitter/receiver result, for the various cases.

PACS numbers: 02.50.-r, 02.70.-c, 89.20.-a

1. Introduction

The statistical physics of disordered systems has been systematically developed over the past few decades to analyse systems of interacting components under different interaction regimes [1, 2]. It enables one to derive typical macroscopic properties of systems comprising a large number of units under conditions of quenched disorder, which correspond to different randomly sampled instances of the problem.

While their origin lies in the study of spin glasses [3, 4, 5], methods of statistical mechanics have been successfully employed to study a broad range of interdisciplinary subjects, from thermodynamics of fluids to biological and even sociological problems. In these studies, the problems were mapped onto known statistical physics models, such as Ising spin systems, and analysed using established methods and techniques from statistical physics.

In particular, these methods have been successfully employed recently to investigate hard computational problems [6, 7] as well as problems in information theory [8] and multi-user communication [9]. They proved to be highly useful for gaining insight into the properties of the problems studied and in providing exact typical case results that complement the rigorous bounds reported in the theoretical computer science and information theory literature.

In the current study we employ the powerful analytical methods of statistical mechanics to examine the typical properties of Multiple-Input Multiple-Output (MIMO) communication channels where messages are encoded using state of the art Low-Density Parity-Check (LDPC) error correcting codes [10, 11, 12, 13].

MIMO channels are becoming increasingly more relevant in modern communication networks that rely on adaptive and ad-hoc configurations. Sensor networks, for instance, may rely on simultaneous transmission of information from a large number of transmitters that give rise to high levels of interference; while multiple access, at various levels, is exercised daily by millions of mobile phone users.

This problem of communication over a MIMO channel is particularly amenable to a statistical physics based analysis for the following reasons: Firstly, previous studies in the areas of LDPC error-correcting codes [8] and Code Division Multiple Access (CDMA) [9, 14] paved the way for the study of MIMO systems; and secondly, the framework of multi-user communication channels is difficult to analyse using traditional methods of information theory [15], but can be readily accommodated within the statistical physics framework, particularly in the case of a large number of users.

The paper is organised as follows: In section 2 we introduce the model to be analysed, followed by statistical physics framework in section 3. We then study several communication channels: a single transmitter and multiple receivers in section 4, multiple access in 5 and symmetric and asymmetric interference channels in section 6. In each of the sections we will consider both cases of a small and large number of users. We conclude with general insights and future directions.

2. The Model

As the communication model considered is based on LDPC codes we will briefly introduce their main characteristics, within the single channel setting, before describing the MIMO communication channel to be studied.

LDPC codes, introduced originally by Gallager [10], are used to encode N-dimensional message vectors $\mathbf{s}$ into M-dimensional codewords $\mathbf{t}$. They are defined by a binary matrix $A = [C_1 \mid C_2]$, called *parity-check matrix*, concatenating two very sparse matrices known to both sender and receiver, with C_2 (of dimensionality $(M-N)\times(M-N)$) being invertible and C_1 of dimensionality $(M-N)\times N$. The matrix A can be either random or structured, characterised by the number of non-zero elements per row/column. Irregular codes show superior performance with respect to regular constructions [11, 16] if they are constructed carefully. However, to simplify the presentation, we focus here on regular constructions; the generalisation of the methods presented here to irregular constructions is straightforward [17, 18].

Encoding refers to the mapping of a N-dimensional binary vector $\mathbf{s} \in \{0,1\}^N$ (original message) to M-dimensional codewords $\mathbf{t} \in \{0,1\}^M$ $(M > N)$ by the linear product

$$\mathbf{t} = G\mathbf{s} \pmod 2 , \tag{1}$$

where all operations are performed in the field $\{0,1\}$ and are indicated by (mod 2). The generator matrix is of the form

$$G = \begin{bmatrix} I \\ C_2^{-1}C_1 \end{bmatrix} \pmod 2 , \tag{2}$$

where I is the $N\times N$ identity matrix. By construction $AG = 0 \pmod 2$ and the first N bits of $\mathbf{t}$ correspond to the original message $\mathbf{s}$.

Decoding is carried out by estimating the most probable transmitted vector from the received corrupted codeword [17, 8].

In this work, we analyse a MIMO Gaussian channel with L sender and O receiver units. In this channel, L original binary messages $s_i \in \{0,1\}^N$, $i = 1, ..., L$ are encoded using LDPC error-correcting codes with *independently chosen* parity-check matrices A_i for each message into binary codewords $t_i \in \{0,1\}^M$.

Note that, both messages s_i and codewords t_i are vectors and should include two different indices, the bit index and a separate index for the number of senders/receivers (i). For brevity, we will reserve the boldface notation for denoting the sets in the sender/receiver indices and will explicitly denote the bit index.

We concentrate here on regular Gallager codes, with exactly K non-zero elements per row and C non-zero elements per column in the parity check matrix, which obey the relation $C = (1-R)K$, where $R = N/M$ is the code rate. The codewords are transmitted in discrete units of time.

In order to apply the tools of statistical mechanics, we use, for mathematical convenience, the transformation

$$x \rightarrow (-1)^x, \tag{3}$$

to map the Boolean variables $t_i \in \{0,1\}^M$ onto spin variables $t_i \in \{1,-1\}^M$. Although they are different variables, we denote both with the same letter t_i. The appropriate use of each one of them will be clear from the context. At each discrete time step μ, the (already mapped) vector $\mathbf{t}^\mu$, $\mu = 1, ..., M$ is transmitted and corrupted by additive white Gaussian noise (AWGN) obeying the equation

$$\mathbf{r}^\mu = S\mathbf{t}^\mu + \boldsymbol{\nu}^\mu, \tag{4}$$

where S is an $O \times L$ matrix with elements S_{ji}, and the Gaussian noise, independent of the time, is given by the vector $\boldsymbol{\nu}^\mu = (\nu_1^\mu, ..., \nu_O^\mu)$ with $\nu_j^\mu \sim \mathcal{N}(0, \sigma_j^2)$, $j = 1, ..., O$, $\forall\mu$, i.e., of zero mean and variance σ_j^2.

The matrix S, which we call the *interference matrix*, plays an essential role in the current analysis as it crosses messages between senders and receivers and is responsible for important interference effects.

3. Replica Analysis

The statistical mechanics based analysis focuses on the decoding process as it is directly linked to the Hamiltonian within the physics framework [19].

Decoding is carried out along the same lines as in LDPC error-correcting codes; the estimate of the first N bits of the codeword, which contain the original uncoded message, will be made by introducing L dynamical variable values $\tau_i \in \{\pm 1\}^M$, representing candidate vectors for each of the transmitted codewords. These will eventually give rise to the estimate of the various codewords $\{t_i\}$, $i = 1, \ldots L$, by the O receivers, each of which has access to all the received messages.

In the statistical analysis, we are interested in the behaviour averaged over the system's disorder, given by the quenched variables $\mathbf{r}$, all possible encodings (or equivalently, all parity-check matrices A_i, for each sender) and all transmitted codewords t_i.

If we allow some degree of error in the decoding, in the form of a prior error probability, the estimator which minimises the bit error probability is the Marginal Posterior Maximiser (MPM) for each dynamical variable [20, 18].

$$\hat{t}_i^{\,\mu} = \mathrm{sgn}\,\langle \tau_i^\mu \rangle_{\mathcal{P}(\boldsymbol{\tau}|\mathbf{r})}, \tag{5}$$

where $\boldsymbol{\tau} = (\tau_1, ..., \tau_L)$.

The expected overlap between the estimated and the transmitted codewords serves as a quality measure for the error correction performance

$$d_i = \frac{1}{M} \sum_{\mu=1}^{M} \left\langle t_i^\mu \mathrm{sgn}\,\langle \tau_i^\mu \rangle_{\mathcal{P}(\boldsymbol{\tau}|\mathbf{r})} \right\rangle_{A_1,...,A_L,\mathbf{r},\mathbf{t}}, \tag{6}$$

where the average is taken over the joint probability distribution $\mathcal{P}(A_1,...,A_L,\mathbf{r},\mathbf{t})$. These performance measures will also be indicative of the dynamical transition from the ferromagnetic solution of perfect decoding to a non-ferromagnetic solution as reflected in their values. Note that the receiver will only get all the messages correctly if $d_i = 1$ for all i at the same time.

The free-energy in the thermodynamic limit $M \to \infty$ is given by

$$f = -\lim_{M\to\infty} \frac{1}{\beta M L} \langle \ln Z \rangle_{A_1,\ldots,A_L,\mathbf{r},\mathbf{t}}, \tag{7}$$

where Z is the partition function

$$Z = \sum_{\boldsymbol{\tau}} \exp\left[-\beta \sum_{j=1}^{O} \mathcal{H}_j(\boldsymbol{\tau}|\mathbf{r})\right],$$

with the Hamiltonian component for each receiver j

$$\mathcal{H}_j(\boldsymbol{\tau}|\mathbf{r}) = \frac{1}{2\sigma_j^2} \sum_{\mu=1}^{M} \left(r_j^\mu - \sum_{i=1}^{L} S_{ji} \tau_i^\mu \right)^2. \tag{8}$$

The Hamiltonian gives rise to a likelihood term for the agreement between the received aggregated vector and the candidate codewords. The decoding temperature β is considered the same for every receiver and each τ_i obeys the parity-check constraint, which for the spin variables is defined by

$$\prod_{\mu=1}^{M} (\tau_i^\mu)^{(A_i)_{\nu\mu}} = 1, \qquad \nu = 1, ..., M-N. \tag{9}$$

The decoding process is aimed at maximising the probability

$$\mathcal{P}(\boldsymbol{\tau}|\mathbf{r}) = \frac{1}{Z} \exp\left[-\beta \sum_{j=1}^{O} \mathcal{H}_j(\boldsymbol{\tau}|\mathbf{r})\right], \tag{10}$$

To calculate $\langle \ln Z \rangle_{A_1,\ldots,A_L,\mathbf{r},\mathbf{t}}$ in the thermodynamic limit, where $M, N \to \infty$ while keeping the code rate $R = N/M$ constant, we use the replica method [1, 2] which relies on the identity

$$\langle \ln Z \rangle = \lim_{n\to 0} \frac{\partial \ln \langle Z^n \rangle}{\partial n}, \tag{11}$$

and employs an analytical continuation of integer values of n to a real value that approaches zero. The calculations will follow the same guidelines as in [18] and we refer the reader to the appendix for further details.

The partition function is given by

$$Z = \sum_{\boldsymbol{\tau}} \left[\prod_{i=1}^{L} \chi(A_i, \tau_i)\right] \exp\left[-\beta \sum_{j=1}^{O} \sum_{\mu=1}^{M} \frac{1}{2\sigma_j^2} \left(r_j^\mu - \sum_{i=1}^{L} S_{ji} \tau_i^\mu \right)^2\right], \tag{12}$$

where χ is an indicator function, which is zero if τ_i does not obey the parity-check equations defined by the matrix A_i.

We assume that the matrices A_i are chosen from the same ensemble of parity-check matrices, which means that all code rates will be the same, $R_i = R$. From information theoretical considerations, the capacity region is then given by

$$\alpha R < \mathcal{C}, \tag{13}$$

where $\alpha \equiv L/O$ is a characteristic constant of the system called its *load* and $\mathcal{C}$, the capacity with joint decoding for an arbitrary distribution of inputs, is obtained by conventional information theoretical methods [15] and is given by

$$\mathcal{C} = \frac{1}{2}\log_2 \det(I_O + SS^T C_\nu^{-1}), \tag{14}$$

where T indicates transposition, I_O is the O-dimensional unit matrix and C_ν is an O-dimensional square diagonal noise matrix given by $(C_\nu)_{jk} = \sigma_j^2 \delta_{jk}$. This result will be used as a benchmark and an upper bound for our results

4. Single Transmitter

In this and the following sections we compare the replica symmetric results with the known information theoretical limits. The case $L = O = 1$ is easily seen to recover the usual results for a simple Gaussian channel as obtained in [18]. In the particular case of one sender and an arbitrary number of receivers, the channel matrix is an O-dimensional column vector. The Replica Symmetric (RS) saddle point equations are (see Appendix A.1)

$$\hat{\pi}(\hat{x}) = \left\langle \delta\left(\hat{x} - \prod_{l=1}^{K-1} x^l \right) \right\rangle_{\mathbf{x}}, \tag{15}$$

$$\pi(x) = \left\langle \delta\left(x - \tanh\left[\sum_{l=1}^{C-1} \operatorname{atanh} \hat{x}^l + \beta \sum_{j=1}^{O} \frac{r_j S_j}{\sigma_j^2} \right] \right) \right\rangle_{\hat{\mathbf{x}},r}, \tag{16}$$

with

$$r \sim \prod_{j=1}^{O} \mathcal{N}(S_j, \sigma_j^2), \tag{17}$$

and where the averages $\langle\rangle_{\mathbf{x}}$ and $\langle\rangle_{\hat{\mathbf{x}}}$ are taken with respect to the distributions $\pi(x)$ and $\hat{\pi}(\hat{x})$, respectively.

The overlap is given by

$$d \quad = \langle \mathrm{sgn}\,(\rho) \rangle_\rho, \quad \text{with} \tag{18}$$

$$\mathcal{P}(\rho) = \left\langle \delta\left(\rho - \tanh\left[\sum_{l=1}^{C} \operatorname{atanh} \hat{x}^l + \beta \sum_{j=1}^{O} \frac{r_j S_j}{\sigma_j^2} \right] \right) \right\rangle_{\hat{\mathbf{x}},r}. \tag{19}$$

The free-energy is

$$\beta f = \frac{C}{K}\ln 2 + C\langle \ln(1 + x\hat{x}) \rangle_{x,\hat{x}} - \frac{C}{K}\left\langle \ln\left(1 + \prod_{m=1}^{K} x^m\right) \right\rangle_{\mathbf{x}}$$

$$-\left\langle \ln\left\{\sum_{\tau=\pm 1}\exp\left[-\sum_{j=1}^{O}\frac{\beta}{2\sigma_j^2}(r_j-S_j\tau)^2\right]\prod_{l=1}^{C}\left(1+\tau\hat{x}^l\right)\right\}\right\rangle_{\hat{\mathbf{x}},r}. \tag{20}$$

The ferromagnetic solution,

$$\hat{\pi}(\hat{x})=\delta(\hat{x}-1), \quad \text{and} \quad \pi(x)=\delta(x-1), \tag{21}$$

represents perfect decoding; it is always present for all noise levels and has free-energy $f=O/2$.

The internal energy and the entropy can be derived from the free energy by the well-known relations

$$u=\frac{\partial}{\partial\beta}(\beta f), \qquad s=\beta(u-f). \tag{22}$$

Let us study the symmetric case where all transmitters emit with the same unit power, all entries of S are equal to 1, and all receivers experience the same noise level σ^2. The capacity, as given by equation (14), is

$$\mathcal{C}=\frac{1}{2}\log_2\left(1+\frac{O}{\sigma^2}\right). \tag{23}$$

and the Shannon limit of perfect decoding is attained when $R=\mathcal{C}$, giving for the threshold noise the result

$$\sigma^2=\frac{O}{2^{2R/O}-1}. \tag{24}$$

To obtain numerical solutions for the various cases we iterated the saddle-point equations (15), using population dynamics, and then calculated the quantities of interest such as the overlap d, the free energy f and the entropy s of equations (18(-(22).

Figure 1 shows the overlap for $L=1$ (one sender), $O=2$ (two receivers), $\sigma_j^2=\sigma^2$ (equal noise level for all receivers), $S_j=1$ and $R=1/4$ (with $K=4$ and $C=3$) at the Nishimori temperature $\beta=1$. The choice of the Nishimori temperature simplifies the analysis as it is known that for this temperature, the system does not enter the spin-glass phase [1]. Similar to the case of LDPC codes, there is no difference between the RS results, obtained using the Nishimori condition, and those obtained using the replica symmetry breaking ansatz for the noisy channel studied here [21, 22]; this motivates our present choice of the replica symmetric ansatz.

We can see that the overlap has the value 1 up to the noise level termed the *dynamical transition* point. This means that while the noise level is kept below this point, all the receivers can perfectly recover the transmitted message as the ferromagnetic solution is the only stable solution. The ferromagnetic solution remains dominant between this point and the *thermodynamical transition point*, which marks the noise level where the non-ferromagnetic state becomes dominant; although an exponential number of sub-optimal stable solutions in this range prevent the iterative population dynamics from converging to the ferromagnetic solution (starting from an arbitrary initial state).

The entropy plot in the inset clarifies the type of solutions obtained as the noise level increases: the entropy is zero up to the dynamical transition, meaning that the only

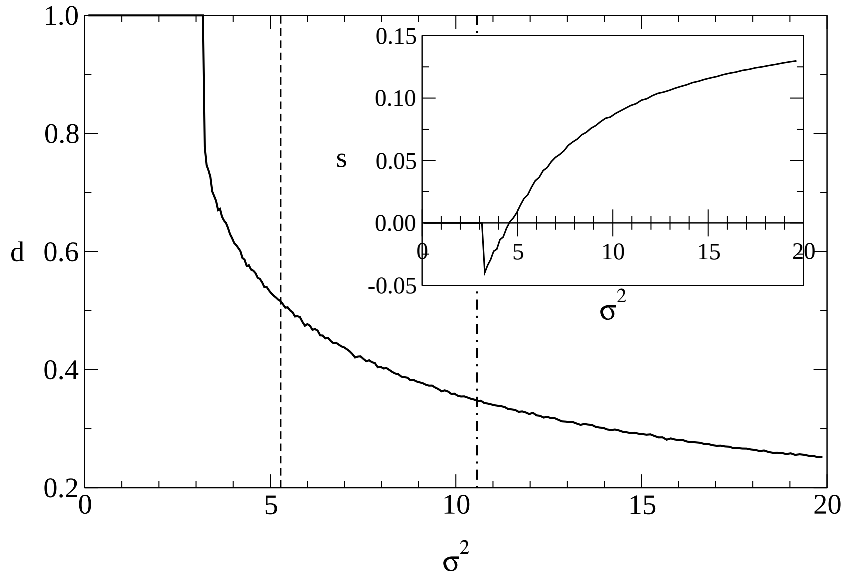

Figure 1. Overlap in the single-sender case for $O = 2$. The solid line describes the result obtained by iterating the saddle point equations (15) from arbitrary initial conditions. The dotted-dashed line shows the theoretical limit obtained from equation (24) and the dashed line shows the theoretical limit for sending a doubled message via a single Gaussian channel. The inset shows a plot of the entropy; the point where the entropy becomes negative marks the emergence of metastable states and the dynamical transition point, while the point where it crosses back the zero entropy line marks the thermodynamical transition noise value.

stable state is the ferromagnetic one. Metastable suboptimal solutions emerge above this point which could be explored using the replica symmetry breaking ansatz [21, 22]; these contribute to (unphysical) negative entropy values in this range [18]. The point where the entropy line crosses the coordinate axis coincides with the *thermodynamical transition* point. The thermodynamical transition is always upper bounded by the Shannon theoretical limit, which is also shown in the overlap plot as a vertical dashed line.

In table 1 we compare the theoretical limit of sending the same message O times via a simple Gaussian channel (one sender and one receiver) with noise level equal to the one considered here (second column) with the theoretical limit for the MIMO channel given by equation (24) (third column) and the points of the dynamical (fourth column) and the thermodynamical (fifth column) transitions obtained by numerical integration of the RS equations for $O = 1, 2, 3$ receivers. It is clear that the dynamical and thermodynamical transitions occur always before the theoretical limit. As expected, the more receivers are added, the higher the noise level the system can tolerate. However, the differences between the dynamical and the thermodynamical transition values, and between the thermodynamical transition and theoretical limit increase. Both are related to the fact that, in adding more receivers, we also increase the number of metastable states in the system; these emerge earlier and contribute to a higher entropy.

Comparing the theoretical noise limit for sending the message O times by a simple Gaussian channel with the limit for the MIMO channel with one sender and O receivers, we can see that the later is just O times the former. This can be understood noting that the information being sent in the MIMO channel is the same as in the O-replicated Gaussian channel, but with O times the power; while in the MIMO channel case, the O bits are sent with power 1 at each time step. We can see by that the results of the RS ansatz that the transition points are even below the theoretical limit for the simple Gaussian channel and significantly below the MIMO limit. This clearly shows that in this type of communication channel, even with joint decoding, the available information is being poorly used. It makes a strong case for the use of *network coding*, i.e., to encode jointly the vectors $\mathbf{t}^\mu$ prior to transmission.

Network coding, for instance using fountain codes [23, 24], is likely to make a better use of the resource by generating codewords that are more suited for better extraction of information under joint decoding.

For $O > 3$ the numerical instabilities grow larger with O and a precise evaluation of the points is increasingly more difficult.

Table 1. Comparison between the Shannon limit for a simple Gaussian channel and the MIMO channel, the dynamical transition point and the thermodynamical transition for the single-sender case ($L = 1$).

O	Shannon's Limit (Gaussian Channel)	Shannon's Limit (MIMO Channel)	Dynamical Transition	Thermodynamical Transition
1	2.41	2.41	1.59	2.24
2	5.28	10.57	3.28	4.59
3	8.17	24.50	4.90	6.68

Another case of interest is that of an infinite number of receivers. When $O \to \infty$, the average over the r variables in equation (15), can be substituted by an average over the Gaussian variable

$$v \equiv \sum_{j=1}^{O} \frac{r_j S_j}{\sigma_j^2} \ . \tag{25}$$

In the case, of equal noise and $S_j = 1$, this variable has zero mean and variance O/σ^2 which reflects the signal to noise ratio appearing in the capacity expression (23).

5. Multiple Access Channel

The multiple access channel (MAC) is a particular case where $O = 1$ and S is an L-dimensional row matrix. Let us consider once more the symmetric case where $S_{ji} = 1$ and $\sigma_j^2 = \sigma^2$. The capacity then becomes

$$\mathcal{C} = \frac{1}{2} \log_2 \left(1 + \frac{L}{\sigma^2} \right), \tag{26}$$

and the threshold noise

$$\sigma^2 = \frac{L}{2^{2LR} - 1}. \tag{27}$$

In this case, due to the interference effect in the received message, one should guarantee that the interference term has the correct order with respect to L. Taking into account that the received messages are independent random variables, we normalise their sum by the factor of $1/\sqrt{L}$.

The simplest case is $L = 2$ and the RS saddle point equations for user 1 are given by

$$\hat{\pi}_1(\hat{x}_1) = \left\langle \delta\left(\hat{x} - \prod_{l=1}^{K-1} x_1^l \right) \right\rangle_{\mathbf{x}}, \tag{28}$$

$$\begin{aligned} \pi_1(x_1) = \Bigg\langle \delta \Bigg(x - \tanh \Bigg\{ \sum_{l=1}^{C-1} \operatorname{atanh} \hat{x}_1^l + \frac{\beta r}{\sigma^2 \sqrt{2}} \\ + \frac{1}{2} \ln \left[\frac{1 - \tanh\left(\frac{\beta}{2\sigma^2}\right) \tanh\left(\sum_{l=1}^{C} \operatorname{atanh} \hat{x}_2^l + \frac{\beta r}{\sigma^2\sqrt{2}} \right)}{1 + \tanh\left(\frac{\beta}{2\sigma^2}\right) \tanh\left(\sum_{l=1}^{C} \operatorname{atanh} \hat{x}_2^l + \frac{\beta r}{\sigma^2\sqrt{2}} \right)} \right] \Bigg\} \Bigg) \Bigg\rangle_{\hat{\mathbf{x}}, r}, \end{aligned} \tag{29}$$

and the overlap is

$$d_1 = \langle \operatorname{sgn}(\rho) \rangle_\rho, \tag{30}$$

$$\begin{aligned} \mathcal{P}(\rho) = \Bigg\langle \delta \Bigg(\rho - \tanh \Bigg\{ \sum_{l=1}^{C} \operatorname{atanh} \hat{x}_1^l + \frac{\beta r}{\sigma^2 \sqrt{2}} \\ + \frac{1}{2} \ln \left[\frac{1 - \tanh\left(\frac{\beta}{2\sigma^2}\right) \tanh\left(\sum_{l=1}^{C} \operatorname{atanh} \hat{x}_2^l + \frac{\beta r}{\sigma^2\sqrt{2}} \right)}{1 + \tanh\left(\frac{\beta}{2\sigma^2}\right) \tanh\left(\sum_{l=1}^{C} \operatorname{atanh} \hat{x}_2^l + \frac{\beta r}{\sigma^2\sqrt{2}} \right)} \right] \Bigg\} \Bigg) \Bigg\rangle_{\hat{\mathbf{x}}, r}, \end{aligned} \tag{31}$$

where

$$r \sim \mathcal{N}\left(\sqrt{2}, \sigma^2\right). \tag{32}$$

The corresponding equations for user 2 are identical to (28)-(31) except for interchanging the indices 1 and 2. The free-energy is given by

$$\begin{aligned} \beta f = \frac{C}{K} \ln 2 + \frac{C}{2} \sum_{i=1}^{2} \langle \ln(1 + x_i \hat{x}_i) \rangle_{x, \hat{x}} - \frac{C}{2K} \sum_{i=1}^{2} \left\langle \ln\left(1 + \prod_{m=1}^{K} x_i^m \right) \right\rangle_{\mathbf{x}} \\ - \frac{1}{2} \left\langle \ln \left\{ \sum_{\tau_1, \tau_2} \exp\left[-\frac{\beta}{2\sigma^2} \left(r - \frac{\tau_1 + \tau_2}{\sqrt{2}} \right)^2 \right] \prod_{i=1}^{2} \prod_{l=1}^{C} (1 + \tau_i \hat{x}_i^l) \right\} \right\rangle_{\hat{\mathbf{x}}, r}. \end{aligned} \tag{33}$$

For the ferromagnetic solution equation (21) results in $f = 0.25$. Indeed, for the MIMO Gaussian channel studied in this paper, we always have that the ferromagnetic free energy is given by $f = 1/2\alpha$.

By iteratively solving the saddle point equations we obtain quantities of interest for this case. The free and internal energies, for $L = 2$ and $R = 1/4$ ($K = 4$ and $C = 3$)

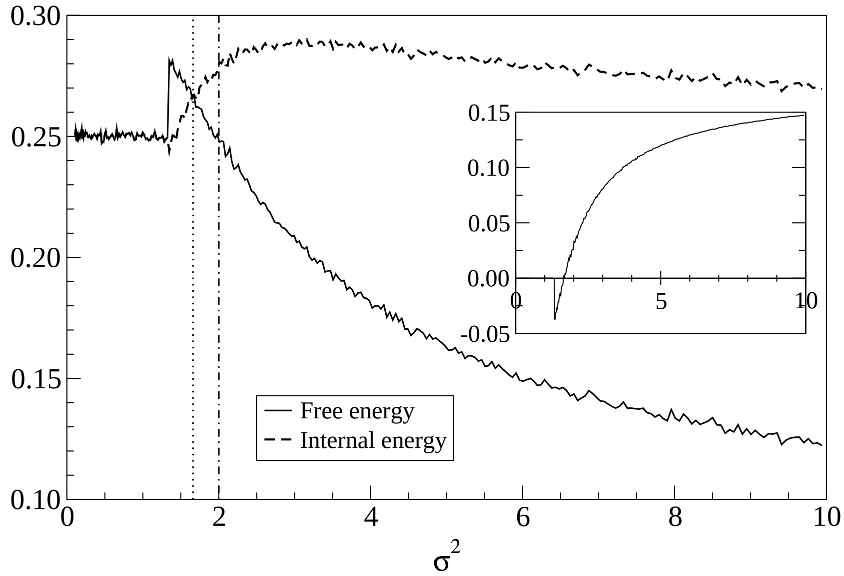

Figure 2. Free energy and internal energy in the MAC case for $L = 2$ represented by the solid and dashed lines, respectively; the results have been obtained by iterating the saddle point equations (15) from arbitrary initial conditions. The dot-dashed line shows the theoretical limit obtained from equation (27) and the dotted line the thermodynamical transition point. The entropy as a function of the noise level is shown in the inset; the point where the entropy becomes negative marks the emergence of metastable states and the dynamical transition point, while the point where it crosses back the zero entropy line marks the thermodynamical transition noise value.

and at the Nishimori temperature, are represented in figure 2 by the solid and dashed lines, respectively; Shannon's theoretical threshold is given by $\sigma^2 = 2$, indicated by the dot-dashed line. The point where the free energy differs from the internal energy, which corresponds to the overlap changing from 1 to lower values, marks the dynamical transition point. The thermodynamical transition point is identified by the crossing of the two energies and is denoted by the dotted line. The entropy function, shown in the inset plotted against the noise level, also helps to identify the dynamical and thermodynamical transition points (where the entropy becomes negative and where it crosses back the coordinate axis, respectively). Both points are below Shannon's limit.

Table 2 shows the results for $L = 1, 2, 3$ senders. The second column gives the theoretical limit obtained from equation (14); it shows the deterioration in performance as the number of senders increases. The deterioration is also evident in the results obtained by numerical results obtained using the RS ansatz given by the dynamical transition (second column) and the thermodynamical transition (third column). Contrary to the single-sender case the difference between the transition points decreases with increasing L; this reflect the fact that additional inputs seem to increase the number sub-optimal solution states (and hence reduce their free energy and affect the thermodynamical transition point) but have a lesser effect on the onset of the metastable states.

Table 2. Comparison between the Shannon's limit, the dynamical transition point and the thermodynamical transition for the MAC case ($O = 1$).

L	Shannon's Limit	Dynamical Transition	Thermodynamical Transition
1	2.41	1.59	2.24
2	2.00	1.32	1.66
3	1.64	1.24	1.45

There are two possible scenarios one may consider in the case of a large number of users ($L \to \infty$). The first is the random interference scenario. Due to the well-known isomorphism between CDMA and MIMO channels, this case is exactly the one calculated in [9] if one rescales $S_{ji} = s_{ji}/\sqrt{L}$ where the s_{ji} are i.i.d. random variables with zero mean, unit variance and vanishing odd moments. The second scenario is the deterministic interference case, where the matrix S is not random. This scenario is of little interest as the capacity grows with the logarithm of the number of users while the transmitted information grows linearly with the number of transmitters; the capacity per user goes to zero in this limit, rendering the communication infeasible.

6. Interference Channel

Interference channel [15] refers to a scenario where several transmitters send data simultaneously to an equal number of receivers; the transmission from a given transmitter to the corresponding receiver is corrupted by (small) interference from all other transmitters. The receivers can then communicate with each other to optimally extract the original messages. Some sensor networks are among the most well known exemplars of systems that could be modelled by an interference channel.

In the following, we will study two basic types of interference channels, the symmetric and the asymmetric case. For simplicity, we limit the number of transmitters and receivers considered here to $L = O = 2$; this will make the interpretation of the results easier and more transparent. Both channels are depicted in figure 3. The symmetric case corresponds to the transmitters sending messages to both receivers (left picture) while in the asymmetric case only the first transmitter sends a message to the first receiver while the second transmitter sends a message to both receivers.

6.1. The Symmetric Interference Channel

We first study the case $L = O = 2$ with a symmetric interference matrix

$$S = \begin{pmatrix} 1 & \epsilon \\ \epsilon & 1 \end{pmatrix}, \tag{34}$$

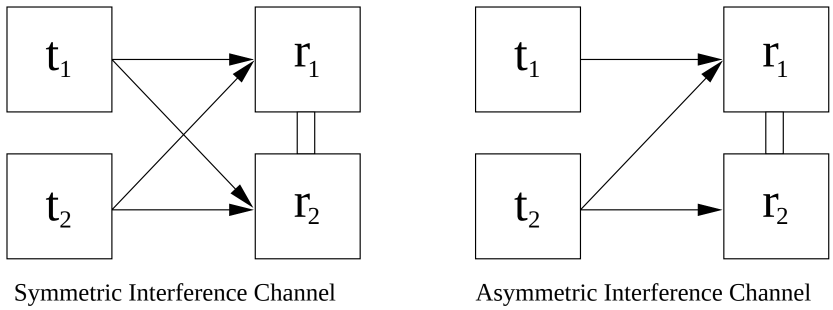

Figure 3. Diagram representing the symmetric (left) and asymmetric (right) interference channels. The first and second transmitters and receivers are denoted by t_1, t_2 and r_1, r_2, respectively. Arrows represent the transmitted messages and the double line bewtween the receivers indicates *joint decoding*.

where $0 < \epsilon \leq 1$. The corresponding capacity can be derived using equation (14) to obtain

$$\mathcal{C} = \frac{1}{2}\log_2\left[1 + \frac{2(1+\epsilon^2)}{\sigma^2} + \frac{(1-\epsilon^2)^2}{\sigma^4}\right]. \tag{35}$$

The RS saddle point equations are given by

$$\hat{\pi}_1(\hat{x}_1) = \left\langle \delta\left(\hat{x}_1 - \prod_{l=1}^{K-1} x_1^l\right)\right\rangle_{\mathbf{x}}, \tag{36}$$

$$\pi_1(x_1) = \left\langle \delta\left(x_1 - \tanh\left\{\sum_{l=1}^{C-1} \operatorname{atanh}\hat{x}_1^l + \frac{\beta}{\sigma^2\sqrt{2}}(r_1 + \epsilon r_2)\right.\right.\right.$$
$$\left.\left.\left. + \ \frac{1}{2}\ln\left[\frac{1 - \tanh(\frac{\beta\epsilon}{\sigma^2})\tanh\left(\frac{\beta(\epsilon r_1 + r_2)}{\sigma^2\sqrt{2}} + \sum_{l=1}^{C}\operatorname{atanh}\hat{x}_2^l\right)}{1 + \tanh(\frac{\beta\epsilon}{\sigma^2})\tanh\left(\frac{\beta(\epsilon r_1 + r_2)}{\sigma^2\sqrt{2}} + \sum_{l=1}^{C}\operatorname{atanh}\hat{x}_2^l\right)}\right]\right\}\right)\right\rangle_{\hat{\mathbf{x}},r}, \tag{37}$$

where

$$r_i \sim \mathcal{N}\left(\frac{1+\epsilon}{\sqrt{2}}, \sigma^2\right), \qquad i = 1, 2. \tag{38}$$

The corresponding equations for $\hat{\pi}_2$ and π_2 are similar to those of $\hat{\pi}_1$ and π_1 and can be obtained by interchanging the indices 1 and 2.

Note that the same scaling as in the MAC case is necessary here due to the interference. However, for $\epsilon = 0$, this scaling should be omitted as the interference vanishes, leaving two separate Gaussian channels.

The overlaps are given by

$$d_i = \langle \operatorname{sgn}(\rho)\rangle_\rho, \tag{39}$$

$$\mathcal{P}(\rho) = \left\langle \delta\left(\rho - \tanh\left\{\sum_{l=1}^{C} \operatorname{atanh}\hat{x}_1^l + \frac{\beta}{\sigma^2\sqrt{2}}(r_1 + \epsilon r_2)\right.\right.\right.$$
$$\left.\left.\left. + \ \frac{1}{2}\ln\left[\frac{1 - \tanh(\frac{\beta\epsilon}{\sigma^2})\tanh\left(\frac{\beta(\epsilon r_1 + r_2)}{\sigma^2\sqrt{2}} + \sum_{l=1}^{C}\operatorname{atanh}\hat{x}_2^l\right)}{1 + \tanh(\frac{\beta\epsilon}{\sigma^2})\tanh\left(\frac{\beta(\epsilon r_1 + r_2)}{\sigma^2\sqrt{2}} + \sum_{l=1}^{C}\operatorname{atanh}\hat{x}_2^l\right)}\right]\right\}\right)\right\rangle_{\hat{\mathbf{x}},r}. \tag{40}$$

The free-energy f is

$$\beta f = \frac{C}{K}\ln 2 + \frac{C}{2}\sum_{i=1}^{2}\langle \ln(1+x_i\hat{x}_i)\rangle_{x,\hat{x}} - \frac{C}{2K}\sum_{i=1}^{2}\left\langle \ln\left(1+\prod_{m=1}^{K} x_i^m\right)\right\rangle_{\mathbf{x}}$$
$$-\frac{1}{2}\left\langle \ln\left\{\sum_{\tau_1,\tau_2}\exp\left[-\frac{\beta}{2\sigma^2}\left(r_1-\frac{\tau_1+\epsilon\tau_2}{\sqrt{2}}\right)^2-\frac{\beta}{2\sigma^2}\left(r_2-\frac{\epsilon\tau_1+\tau_2}{\sqrt{2}}\right)^2\right]\right.\right.$$
$$\left.\left.\times\prod_{i=1}^{2}\prod_{l=1}^{C}\left(1+\tau_i\hat{x}_i^l\right)\right\}\right\rangle_{\hat{\mathbf{x}},r}. \qquad (41)$$

Accordingly, the free-energy of the ferromagnetic solution (21) is $f = 0.5$, as for the simple Gaussian channel.

We solved numerically the saddle point equations (36) and calculated quantities of relevance in this case. The graphs for the overlap, entropy and energy are qualitatively the same as in the other two cases, with a similar behaviour with the appearance of both dynamical and thermodynamical transition points before Shannon's limit.

Figures 4 and 5 show the field distributions $\pi(x)$ and $\hat{\pi}(\hat{x})$, respectively, for four different values of the noise level in the RS ansatz; with $\epsilon = 1.0$, $\beta = 1$ and $R = 1/4$ ($K = 4$, $C = 3$). It should be noticed that, before the dynamical transition point, these distributions are delta functions centred at 1, corresponding to the ferromagnetic solution (21). The plotted distributions are histograms with 500 bins for 40000 fields. In figure 4 we see how the π distribution changes slowly from the delta function in 1 to a delta function in zero, which is the solution for $\sigma^2 \to \infty$. The $\hat{\pi}$ distribution depicted in figure 5 changes abruptly from the delta function in 1 to a highly peaked asymmetric distribution around zero (paramagnetic solution) when the dynamical transition point is crossed. Looking at the values on each of the graphs, it is visible how the scales increase very fast as the noise level attains higher values.

If one keep a constant code rate $R = 1/4$ but allows ϵ to vary, one obtains the dependence of the threshold noise as a function of ϵ, depicted in figure 6 (for $\beta = 1$, $K = 4$ and $C = 3$). Both dynamical (dashed line) and thermodynamical transition values (dashed-dotted line) are upper bounded by the theoretical limit. Although this may seem counterintuitive, the communication resilience against noise increases with the interference level. This can be understood in the case of joint detection by noting that the increased interference provides more information about the other transmitters, such that higher levels of noise can be tolerated by joint decoding.

For large O with $L \sim \mathcal{O}(1)$ or large L with $O \sim \mathcal{O}(1)$, the results should approach those obtained for large number of users in the single transmitter and in the MAC case, respectively. The behaviour must be dictated by the value of the system load α. In this case, we expect the results to cross from a behaviour similar to the one of a MAC channel for $\alpha > 1$ to one that resembles the single transmitter case for $\alpha < 1$. We are currently working on the analytical and computational aspects of this last case as well as on the case of large O and L values while keeping the ration $L/O \sim \mathcal{O}(1)$ finite.

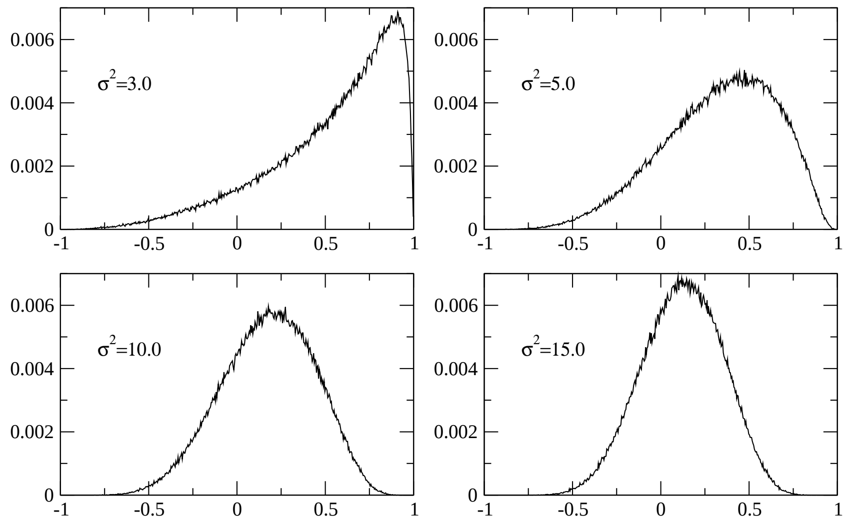

Figure 4. Profile of the π distribution. The plots are histograms with 500 bins for a population of 40000 fields. The noise level value σ^2 is indicated in each graph. All noise levels are above the dynamical transition point; below the transition point the distribution is a delta function $\delta(x-1)$. Note how the distribution changes slowly from $\delta(x-1)$ to $\delta(x)$ as the noise level increases.

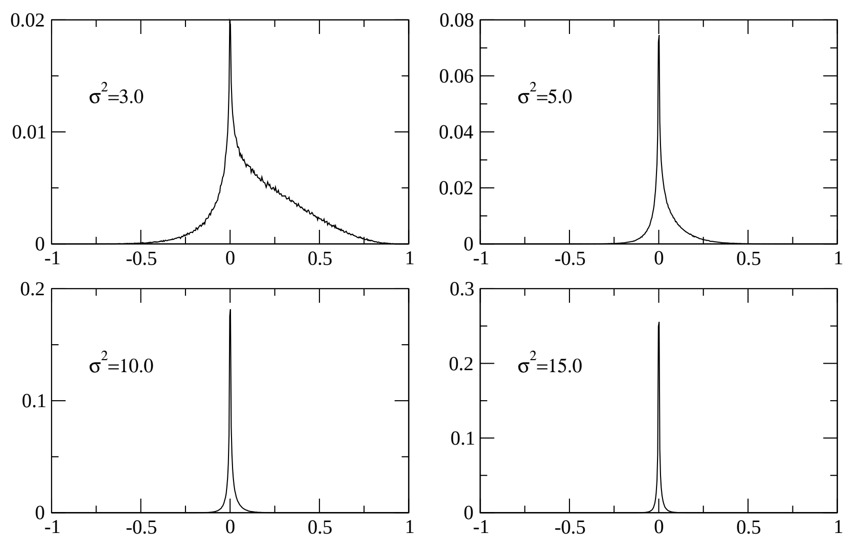

Figure 5. Profile of the $\hat{\pi}$ distribution. The plots are histograms with 500 bins for a population of 40000 fields. The noise level value σ^2 is indicated in each graph. All noise levels are above the dynamical transition point; below it the profile distribution is simply a delta function $\delta(\hat{x}-1)$. In this case, the profile changes abruptly from $\delta(\hat{x}-1)$ to an asymmetric distribution centred at $\hat{x}=0$ and diverges rapidly to $\delta(\hat{x})$ with the increasing noise.

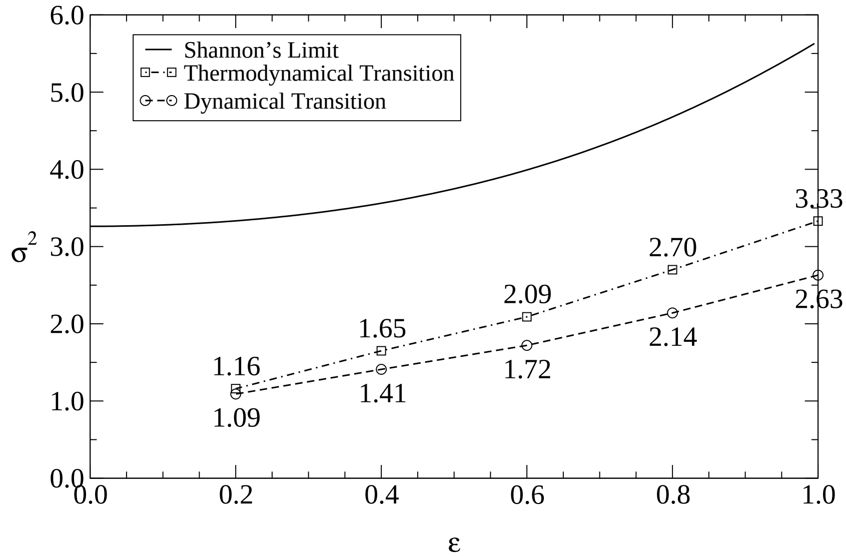

Figure 6. Transition points and theoretical limits as a function of the interference level ϵ. The solid line represents the theoretical limit obtained from information theoretical methods; the dashed-dotted and dashed lines correspond to the thermodynamical and dynamical transition points, respectively.

6.2. The Asymmetric Interference Channel

A variant of the interference channel discussed in section 6.1, for the case of $L = O = 2$, is the asymmetric interference channel. This realisation of the interference channel is highly relevant to cases where receivers are distributed at random and experience different noise levels, for instance, in the case of sensor networks. The interference matrix is asymmetric in this case and takes the form (for $L = O = 2$)

$$S = \begin{pmatrix} 1 & \epsilon \\ 0 & 1 \end{pmatrix}, \tag{42}$$

with $0 < \epsilon \leq 1$. The corresponding capacity is now (again by (14))

$$\mathcal{C} = \frac{1}{2}\log_2\left[1 + \frac{(2+\epsilon^2)}{\sigma^2} + \frac{1}{\sigma^4}\right]. \tag{43}$$

The RS saddle point equations are given by

$$\hat{\pi}_i(\hat{x}_i) = \left\langle \delta\left(\hat{x}_i - \prod_{l=1}^{K-1} x_i^l\right)\right\rangle_{\mathbf{x}}, \qquad i = 1, 2, \tag{44}$$

$$\pi_1(x_1) = \left\langle \delta\left(x_1 - \tanh\left\{\sum_{l=1}^{C-1} \operatorname{atanh}\hat{x}_1^l + \frac{\beta r_1}{\sigma^2\sqrt{2}}\right.\right.\right.$$
$$\left.\left.\left. + \ \frac{1}{2}\ln\left[\frac{1 - \tanh(\frac{\beta\epsilon}{2\sigma^2})\tanh\left(\frac{\beta\epsilon r_1}{\sigma^2\sqrt{2}} + \frac{\beta r_2}{\sigma^2} + \sum_{l=1}^{C}\operatorname{atanh}\hat{x}_2^l\right)}{1 + \tanh(\frac{\beta\epsilon}{2\sigma^2})\tanh\left(\frac{\beta\epsilon r_1}{\sigma^2\sqrt{2}} + \frac{\beta r_2}{\sigma^2} + \sum_{l=1}^{C}\operatorname{atanh}\hat{x}_2^l\right)}\right]\right\}\right)\right\rangle_{\hat{\mathbf{x}},r} \tag{45}$$

$$\pi_2(x_2) = \left\langle \delta\left(x_2 - \tanh\left\{\sum_{l=1}^{C-1} \operatorname{atanh}\hat{x}_2^l + \frac{\beta\epsilon r_1}{\sigma^2\sqrt{2}} + \frac{\beta r_2}{\sigma^2}\right.\right.\right.$$

$$+\ \frac{1}{2}\ln\left[\frac{1-\tanh(\frac{\beta\epsilon}{2\sigma^2})\tanh\left(\frac{\beta r_1}{\sigma^2\sqrt{2}}+\sum_{l=1}^{C}\operatorname{atanh}\hat{x}_1^l\right)}{1+\tanh(\frac{\beta\epsilon}{2\sigma^2})\tanh\left(\frac{\beta r_1}{\sigma^2\sqrt{2}}+\sum_{l=1}^{C}\operatorname{atanh}\hat{x}_1^l\right)}\right]\Bigg\}\Bigg)\Bigg\rangle_{\hat{\mathbf{x}},r}, \tag{46}$$

where

$$r_1 \sim \mathcal{N}\left(\frac{1+\epsilon}{\sqrt{2}},\sigma^2\right), \qquad r_2 \sim \mathcal{N}\left(1,\sigma^2\right). \tag{47}$$

In this case, the scaling $1/\sqrt{L}$ (in this case $L=2$, although the treatment can be extended to include a general number of sources) appears only in the first receiver, as it is being affected by the interference.

The overlaps are given by

$$d_i = \langle \operatorname{sgn}(\rho_i)\rangle_{\rho_i}, \qquad i=1,2, \tag{48}$$

$$\mathcal{P}(\rho_1) = \Bigg\langle \delta\Bigg(\rho_1 - \tanh\Bigg\{\sum_{l=1}^{C}\operatorname{atanh}\hat{x}_1^l + \frac{\beta r_1}{\sigma^2\sqrt{2}}$$
$$+\ \frac{1}{2}\ln\left[\frac{1-\tanh(\frac{\beta\epsilon}{2\sigma^2})\tanh\left(\frac{\beta\epsilon r_1}{\sigma^2\sqrt{2}}+\frac{\beta r_2}{\sigma^2}+\sum_{l=1}^{C}\operatorname{atanh}\hat{x}_2^l\right)}{1+\tanh(\frac{\beta\epsilon}{2\sigma^2})\tanh\left(\frac{\beta\epsilon r_1}{\sigma^2\sqrt{2}}+\frac{\beta r_2}{\sigma^2}+\sum_{l=1}^{C}\operatorname{atanh}\hat{x}_2^l\right)}\right]\Bigg\}\Bigg)\Bigg\rangle_{\hat{\mathbf{x}},r} \tag{49}$$

$$\mathcal{P}(\rho_2) = \Bigg\langle \delta\Bigg(\rho_2 - \tanh\Bigg\{\sum_{l=1}^{C}\operatorname{atanh}\hat{x}_2^l + \frac{\beta\epsilon r_1}{\sigma^2\sqrt{2}} + \frac{\beta r_2}{\sigma^2}$$
$$+\ \frac{1}{2}\ln\left[\frac{1-\tanh(\frac{\beta\epsilon}{2\sigma^2})\tanh\left(\frac{\beta r_1}{\sigma^2\sqrt{2}}+\sum_{l=1}^{C}\operatorname{atanh}\hat{x}_1^l\right)}{1+\tanh(\frac{\beta\epsilon}{2\sigma^2})\tanh\left(\frac{\beta r_1}{\sigma^2\sqrt{2}}+\sum_{l=1}^{C}\operatorname{atanh}\hat{x}_1^l\right)}\right]\Bigg\}\Bigg)\Bigg\rangle_{\hat{\mathbf{x}},r}, \tag{50}$$

The free-energy f is obtained from

$$\beta f = \frac{C}{K}\ln 2 + \frac{C}{2}\sum_{i=1}^{2}\langle \ln(1+x_i\hat{x}_i)\rangle_{x,\hat{x}} - \frac{C}{2K}\sum_{i=1}^{2}\left\langle \ln\left(1+\prod_{m=1}^{K}x_i^m\right)\right\rangle_{\mathbf{x}}$$
$$-\frac{1}{2}\Bigg\langle \ln\Bigg\{\sum_{\tau_1,\tau_2}\exp\left[-\frac{\beta}{2\sigma^2}\left(r_1-\frac{\tau_1+\epsilon\tau_2}{\sqrt{2}}\right)^2-\frac{\beta}{2\sigma^2}(r_2-\tau_2)^2\right]$$
$$\times\prod_{i=1}^{2}\prod_{l=1}^{C}\left(1+\tau_i\hat{x}_i^l\right)\Bigg\}\Bigg\rangle_{\hat{\mathbf{x}},r}, \tag{51}$$

with the free energy of the ferromagnetic solution $f=0.5$.

The numerical solution of (44) with $\epsilon=1.0$, $\beta=1$ and $R=1/4$ ($K=4$, $C=3$) leads to the results depicted in figure 7. The top plot shows the overlaps of the solutions obtained for both receivers. Interestingly, the overlaps for the two receivers behave significantly differently in spite of the fact that messages are decoded jointly; this one of the striking features of the asymmetric interference channel. The overlap for both receivers is one up to the point where the first receiver (thick continuous line), which experiences interference effects, exhibits a dynamical transition which signals the practical noise threshold for this system. The same point can be identified in the entropy plot (bottom right) as the point where the entropy becomes negative. This point is very far from Shannon's limit (dotted line) $\sigma^2 \approx 7.56$; this can be explained by the additional metastable states introduced by the asymmetric interference. Note that the first receiver undergoes a (dynamical) transition before the second receiver (thick dashed line) that does not suffer from interference; this is in spite of the fact that the messages are decoded jointly.

However, the dynamical transition point for the second receiver introduces an unexpected behaviour at the first receiver. When the overlap for the second receiver drops to sub-optimal levels, the first receiver exhibits a sudden *increase* in its decoding overlap. This behaviour may be understood by examining the average overlap, which can be viewed as the overlap for the entire system. We see that the system's overlap suffers a second transition at this point, although the average overlap continues to decrease monotonically; the *system as a whole* has a certain amount of retrievable information which keeps decreasing with the noise level.

The above result shows that the way information is distributed among the receivers can be highly non-trivial. It also shows that for systems with many users, the thermodynamical transition point is determined mostly by the weakest node (which experiences the highest levels of interference) and may lead practical limits that are very far from the Shannon bound.

7. Conclusions

We investigated the properties of coded Gaussian MIMO channels using methods of statistical mechanics. The problems investigated relate to the cases of a single transmitter, multiple access and interference in the case of multiple receivers and transmitters. In all cases, transmissions are coded using LDPC error-correcting codes.

The method used in the analysis, the replica approach, enables one to obtain typical case results that complements the theoretical bounds reported in the information theory literature. The numerical results obtained for particular MIMO channels and parameter values are presented and contrasted with the information theoretical results.

MIMO channels are characterised by an interference matrix S which mixes inputs from the various transmitters to provide the messages at the receiving end. We examine cases where the interference matrix is deterministic. This requires the introduction of a non-trivial scaling in order to obtain meaningful results.

The results obtained provide characteristic, typical case, results in all cases. For the single transmitter and MAC problems we show both dynamical and thermodynamical transition points as functions of the number of receivers and transmitters, respectively. We see that the gaps between the practical and theoretical thresholds (dynamical and thermodynamical transitions, respectively), and the gap between them and Shannon's limit, increase with the number of receivers in the single transmitter case and decrease with the number of transmitters in the MAC case.

In the single transmitter case, this results from the increase in the number of

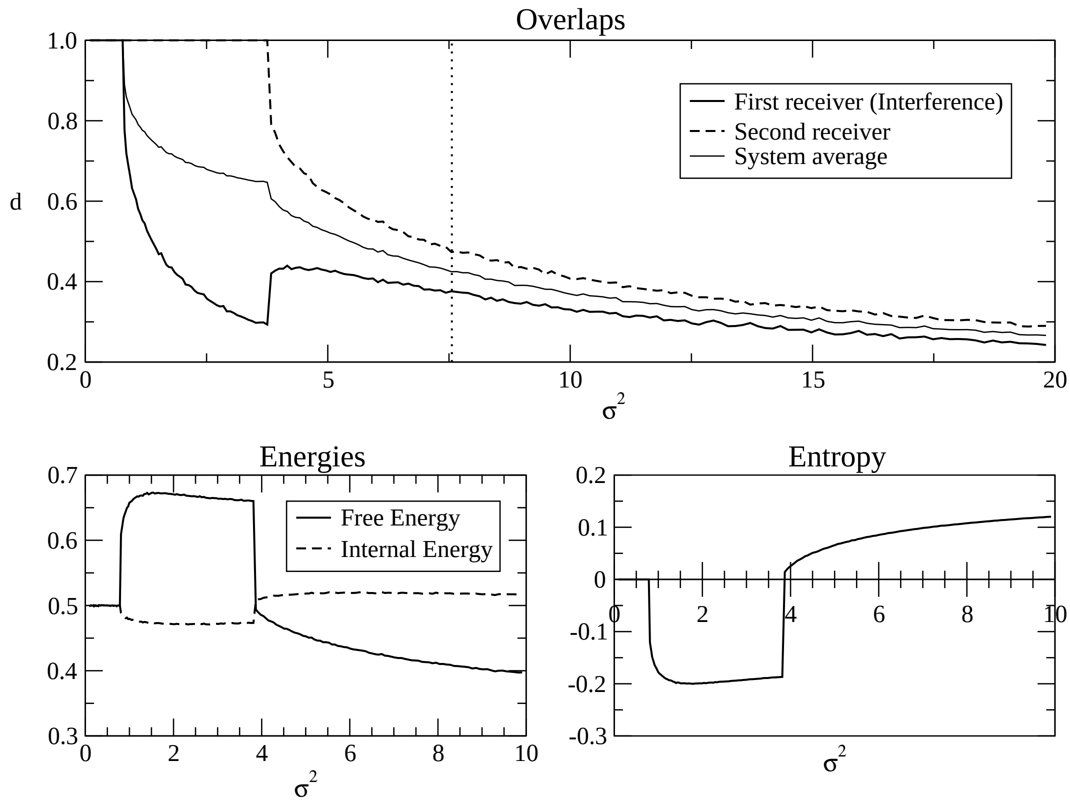

Figure 7. Numerical integration of saddle point equations for the asymmetric interference channel. The upper plot shows the overlap for the first receiver (thick continuous line), which suffer the effects of interference, the second receiver (thick dashed line) and the average overlap for the entire system (thin continuous line). The Shannon limit for the system is depicted by the dotted vertical line. At the bottom, the left graph shows the free-energy (continuous line) and the internal energy (dashed line) for the entire systems while the right graph shows the entropy values obtained under the RS ansatz.

variables and consequentially the increase in the number of metastable states. The point where metastable solutions emerge determines the dynamical transition point (practical threshold), while the number of metastable states affects the thermodynamic transition point. The increasing number of transmitters in the MAC case enables one to effectively reduce the noise level by averaging over a higher number of random and independent noise sources.

The comparison with theoretical limits for the single transmitter case reveals an important feature of multiuser channels as to how the available information is used. The huge gap between the transition points and Shannon's limit is indicative of a poor use of resource, and suggests network coding as a measure to achieve a good use of resource; without it, the system's efficiency remains below the achievable theoretical limit for sending the same message repeatedly via a simple Gaussian channel. One possible solution that we are currently investigating is the use of fountain codes [23, 24] for making a more efficient use of the available resource.

The main result in the symmetric interference channel case is the increase in both dynamical and thermodynamical transition points as a function of the interference parameter ϵ. Results for low ϵ values are similar to the case of separate Gaussian channels; as ϵ increases, both values come closer to Shannon's theoretical limit with the thermodynamical transition point showing a stronger increase. This could be explained by the increase of (mixed) information in comparison to the noise level; this information can be decoded jointly, with an effectively lower noise level. The more moderate increase in the practical threshold (dynamical transition) is due to the difficulty in jointly decoding the various sources in practice due to the emergence of metastable states.

In the asymmetric case we found a striking different behaviour of the system. The new feature observed is the second transition suffered by the system as a whole. We also detected a surprising behaviour of the receiver which experiences interference; in spite of the joint decoding, the information available to it is suppressed by the second receiver. Only when the second receiver stops decoding perfectly, the performance of the first receiver improves.

An interesting extension, of significant practical relevance, would be the extend the LDPC coding framework to complex MIMO channels, where circular noise is considered [25]. Another as well as the possible extension is the case of a large number of senders and receivers where the ration between them remains finite. The study of these and other related problems is underway.

Acknowledgements

Support from EVERGROW, IP No. 1935 in FP6 of the EU is gratefully acknowledged.

References

[1] Nishimori, H. *Statistical Physics of Spin Glasses and Information Processing.* Oxford University Press, Oxford, UK, (2001).
[2] Mézard, M., Parisi, G., and Virasoro, M. *Spin Glass Theory and Beyond.* World Scientific Publishing Co., Singapore, (1987).
[3] Edwards, S. F. and Anderson, P. W. *J. Phys. F: Metal Phys.* **5**, 965–974 (1975).
[4] Sherrington, D. and Kirkpatrick, S. *Phys. Rev. Lett.* **35**, 1792–1796 (1975).
[5] Kirkpatrick, S. and Sherrington, D. *Phys. Rev. B* **17**, 4384–4403 (1978).
[6] Monasson, R. and Zecchina, R. *Phys. Rev. Lett.* **76**, 3881–3885 (1996).
[7] Hartmann, A. K. and Weigt, M. *Phase Transitions in Combinatorial Optimization Problems: Basics, Algorithms and Statistical Mechanics.* Wiley-VCH, (2005).
[8] Kabashima, Y. and Saad, D. *J. Phys. A.* **37**, R1–R43 (2004).
[9] Tanaka, T. *IEEE Trans. Inform. Theory* **11**, 2888–2910 (2002).
[10] Gallager, R. *IRE Trans. Info. Theory* **IT-8**, 21–28 (1962).
[11] Richardson, T., Shokrollahi, A., and Urbanke, R. *IEEE Trans. on Info. Theory* **47**, 619–637 (2001).
[12] Richardson, T. and Urbanke, R. *IEEE Trans. on Info. Theory* **47**, 599–618 (2001).
[13] MacKay, D. *Information Theory, Inference and Learning Algorithms.* Cambridge University Press, Cambridge, MA, (2003). available at http://wol.ra.phy.cam.ac.uk/mackay/.
[14] Tanaka, T. and Saad, D. Technical report, (2003). unpublished.

[15] Cover, T. and Thomas, J. *Elements of Information Theory.* John Wiley & Sons, New York, NY, (1991).
[16] Kanter, I. and Saad, D. *Phys. Rev. Lett.* **83**, 2660–2663 (1999).
[17] Vicente, R., Saad, D., and Kabashima, Y. In *Advances in Imaging and Electron Physics,* Hawkes, P., editor, volume 125, 232–353. Academic Press (2002).
[18] Vicente, R., Saad, D., and Kabashima, Y. *J. Phys. A* **33**, 6527–6542 (2000).
[19] Sourlas, N. *Europhys. Lett.* **25**, 159–164 (1994).
[20] Iba, Y. *J. Phys. A* **32**, 3875–3888 (1999).
[21] Franz, S., Leone, M., Montanari, A., and Ricci-Tersenghi, F. *Phys. Rev. E* **66**, 046120 (2002).
[22] Migliorini, G. and Saad, D. *Phys. Rev. E* **73**, 026122 (2006).
[23] Luby, M. In *in Proc. of The 43rd Annual IEEE Symposium on Foundation of Computer Science*, 271–282, (2002).
[24] Luby, M. G., Mitzenmacher, M., Shokrollahi, M. A., Spielman, D. A., and Stemann, V. In *Proc. of the 29th annual ACM symposium on Theory of computing*, 150–159, (1997).
[25] Moustakas, A. L., Simon, S. H., and Sengupta, A. M. *IEEE Transactions on Information Theory* **49**, 2545–2561 (2003).

Appendix A. Replica Symmetric Calculations

¿From the partition function (12), we can write the averaged replicated partition function $\mathcal{Z}_n \equiv \langle Z^n \rangle_{A_1,\ldots,A_L,\mathbf{r},\mathbf{t}}$ as

$$\mathcal{Z}_n = \frac{\lambda^M}{2^{NL}} \sum_{\{\tau_a\}} \int d\mathbf{r}\, \exp\left[-\sum_{j=1}^{O}\sum_{\mu=1}^{M} \frac{1}{2\sigma_j^2}\left(r_j^\mu - \sum_{i=1}^{L} S_{ji}\tau_{i0}^\mu\right)^2\right]$$
$$\times \exp\left[-\sum_{a=1}^{n}\sum_{j=1}^{O}\sum_{\mu=1}^{M} \frac{\beta}{2\sigma_j^2}\left(r_j^\mu - \sum_{i=1}^{L} S_{ji}\tau_{ia}^\mu\right)^2\right]\left[\prod_{i=1}^{L}\Lambda_i(\{\tau_{ia}\})\right], \tag{A.1}$$

$$\lambda \equiv \prod_{j=1}^{O}(2\pi\sigma_j^2)^{-1/2}, \tag{A.2}$$

where the multiplicative constants come from the normalisation of the probability distributions in the outside average and we defined $\tau_{i0} \equiv t_i$. Following [14], we have

$$\Lambda_i(\{\tau_{ia}\}) \equiv \left\langle \prod_{a=0}^{n} \chi(A_i, \tau_{ia}) \right\rangle_{A_i}$$
$$= \frac{1}{N_A} \oint D\mathbf{Z}_i \left[\sum_{\omega_i}\left(\frac{1}{M}\sum_{\mu} Z_i^\mu \tau_{ia_1^i}^\mu \cdots \tau_{ia_{m_i}^i}^\mu\right)^K\right]^{M-N}, \tag{A.3}$$

where

$$D\mathbf{Z}_i \equiv \left(\frac{1}{2^{M-N}}\right)^{n+1} \prod_{\mu=1}^{M} \frac{dZ_i^\mu}{2\pi i}\frac{1}{(Z_i^\mu)^{C+1}}, \qquad \omega_i \equiv < a_1^i \cdots a_{m_i}^i >, \tag{A.4}$$

and the variables m_i assume all integer values for the index i from 0 to $n+1$.

Defining

$$q_{\omega_i} \equiv \frac{1}{M}\sum_{\mu} Z_i^\mu \tau_{ia_1^i}^\mu \cdots \tau_{ia_{m_i}^i}^\mu, \tag{A.5}$$

and using integral representations for the delta functions, we can write

$$\begin{aligned}\mathcal{Z}_n = 2^{-NL} \int \left(\prod_{i=1}^{L} \prod_{\omega_i} \frac{dq_{\omega_i} d\hat{q}_{\omega_i}}{2\pi i/M} \right) \left[\prod_{i=1}^{L} \sum_{\omega_i} (q_{\omega_i})^K \right]^{M-N} \\ \times \prod_{i=1}^{L} \exp\left(-M \sum_{\omega_i} q_{\omega_i} \hat{q}_{\omega_i} \right) \\ \times \sum_{\{\tau_a\}} \prod_{i=1}^{L} \left[\oint D\mathbf{Z}_i \exp\left(\sum_{\omega_i} \hat{q}_{\omega_i} \sum_{\mu} Z_i^{\mu} \tau^{\mu}_{ia^i_1} \cdots \tau^{\mu}_{ia^i_{m_i}} \right) \right] \\ \times \lambda^M \int d\mathbf{r} \, \exp\left[- \sum_{j=1}^{O} \sum_{\mu=1}^{M} \frac{1}{2\sigma_j^2} \left(r_j^{\mu} - \sum_{i=1}^{L} S_{ji} \tau^{\mu}_{i0} \right)^2 \right] \\ \times \exp\left[- \sum_{a=1}^{n} \sum_{j=1}^{O} \sum_{\mu=1}^{M} \frac{\beta}{2\sigma_j^2} \left(r_j^{\mu} - \sum_{i=1}^{L} S_{ji} \tau^{\mu}_{ia} \right)^2 \right]. \end{aligned} \tag{A.6}$$

Defining

$$\prod_{i=1}^{L} \prod_{\omega_i} \frac{dq_{\omega_i} d\hat{q}_{\omega_i}}{2\pi i/M} \equiv DqD\hat{q}, \tag{A.7}$$

and

$$\gamma = \frac{2^{-(M-N)(n+1)} 2^{-N}}{N_A}, \tag{A.8}$$

and integrating over the variables Z_i^{μ}, the μ indices factorise and we obtain

$$\mathcal{Z}_n = \int DqD\hat{q} \, \exp\left[ML\tilde{f}(q,\hat{q}) \right], \tag{A.9}$$

with

$$\begin{aligned}\tilde{f}(q,\hat{q}) \equiv \frac{1}{M} \ln\gamma + \frac{(1-R)}{L} \sum_{i=1}^{L} \ln\left[\sum_{\omega_i} (q_{\omega_i})^K \right] \\ - \frac{1}{L} \sum_{i=1}^{L} \sum_{\omega_i} q_{\omega_i} \hat{q}_{\omega_i} + \frac{1}{L} \ln\Phi, \end{aligned} \tag{A.10}$$

and

$$\begin{aligned}\Phi \equiv \lambda \int d^L r \sum_{\{\tau_a\}} \left[\prod_{i=1}^{L} \frac{1}{C!} \left(\sum_{\omega_i} \hat{q}_{\omega_i} \tau_{ia^i_1} \cdots \tau_{ia^i_{m_i}} \right)^C \right] \\ \times \exp\left[- \sum_{j=1}^{O} \frac{1}{2\sigma_j^2} \left(r_j - \sum_{i=1}^{L} S_{ji} \tau_{i0} \right)^2 \right] \\ \times \exp\left[- \sum_{a=1}^{n} \sum_{j=1}^{O} \frac{\beta}{2\sigma_j^2} \left(r_j - \sum_{i=1}^{L} S_{ji} \tau_{ia} \right)^2 \right]. \end{aligned} \tag{A.11}$$

Using the replica symmetric (RS) ansatz

$$
\begin{aligned}
q_{\omega_i} &= q_0^i \Big\langle (x_i)^{m_i-\Delta_i} \Big\rangle_{x_i}, \qquad x_i \sim \pi_i(x_i), \\
\hat{q}_{\omega_i} &= \hat{q}_0^i \Big\langle (\hat{x}_i)^{m_i-\Delta_i} \Big\rangle_{\hat{x}_i}, \qquad \hat{x}_i \sim \hat{\pi}_i(\hat{x}_i),
\end{aligned}
\tag{A.12}
$$

where

$$
\Delta_i = \begin{cases} 1, & 0 \in \{a_1^i, ..., a_{m_i}^i\} \\ 0, & \text{otherwise.} \end{cases}
\tag{A.13}
$$

For small n

$$
\ln\left[\sum_{\omega_i} (q_{\omega_i})^K\right] = \ln\left[2(q_0^i)^K\right] + n\left\langle \ln\left(1 + \prod_{m=1}^{K} x_i^m\right)\right\rangle_{\mathbf{x}},
\tag{A.14}
$$

where $\langle\cdot\rangle_{\mathbf{x}}$ indicates the average over all variables x_i^m and

$$
\sum_{\omega_i} q_{\omega_i}\hat{q}_{\omega_i} = 2q_0^i\hat{q}_0^i\Big[1 + n\langle\ln(1 + x_i\hat{x}_i)\rangle_{x_i,\hat{x}_i}\Big],
\tag{A.15}
$$

$$
\sum_{\omega_i} \hat{q}_{\omega_i}\tau^{\mu}_{ia_1^i}\cdots\tau^{\mu}_{ia_{m_i}^i} = \hat{q}_0^i(1+\tau_{i0})\left\langle \prod_{a=1}^{n}(1+\tau_{ia}\hat{x}_i)\right\rangle_{\hat{\mathbf{x}}}.
\tag{A.16}
$$

Inserting the result in Φ and summing over the zero-th replicas we have

$$
\begin{aligned}
\Phi = \frac{\left(2^L\hat{Q}_0\right)^C}{(C!)^L} \Bigg\langle & \sum_{\{\tau_a\}} \prod_{l=1}^{C}\prod_{a=1}^{n}\prod_{i=1}^{L}(1+\tau_{ia}\hat{x}_i^l) \\
& \times \exp\left[-\sum_{a=1}^{n}\sum_{j=1}^{O}\frac{\beta}{2\sigma_j^2}\left(r_j - \sum_{i=1}^{L}S_{ji}\tau_{ia}\right)^2\right]\Bigg\rangle_{r,\hat{\mathbf{x}}}.
\end{aligned}
\tag{A.17}
$$

where $\hat{Q}_0 \equiv \prod_i \hat{q}_0^i$ and

$$
r \sim \prod_{j=1}^{O}\mathcal{N}\left(\sum_{i=1}^{L}S_{ji}, \sigma_j^2\right).
\tag{A.18}
$$

The sum over the n replicas factorises to

$$
\begin{aligned}
\Phi = \frac{\left(2^L\hat{Q}_0\right)^C}{(C!)^L} \Bigg\langle \Bigg\{ & \sum_{\tau_1,\ldots,\tau_L} \prod_{l=1}^{C}\prod_{i=1}^{L}(1+\tau_i\hat{x}_i^l) \\
\times \exp & \left[-\sum_{j=1}^{O}\frac{\beta}{2\sigma_j^2}\left(r_j - \sum_{i=1}^{L}S_{ji}\tau_i\right)^2\right]\Bigg\}^n\Bigg\rangle_{r,\hat{\mathbf{x}}}.
\end{aligned}
\tag{A.19}
$$

Appendix A.1. Single Transmitter

Let us consider $L = 1$. Then

$$\Phi = \frac{(2\hat{q}_0)^C}{C!} \left\langle \left\{ \sum_{\tau} \prod_{l=1}^{C} \left(1 + \tau \hat{x}^l\right) \times \exp\left[- \sum_{j=1}^{O} \frac{\beta}{2\sigma_j^2} (r_j - S_j \tau)^2 \right] \right\}^n \right\rangle_{r,\hat{\mathbf{x}}} . \tag{A.20}$$

and, for small n

$$\ln \Phi = \ln \frac{(2\hat{q}_0)^C}{C!} + n \left\langle \ln \left\{ \sum_{\tau} \prod_{l=1}^{C} \left(1 + \tau \hat{x}^l\right) \exp\left[- \sum_{j=1}^{O} \frac{\beta}{2\sigma_j^2} (r_j - S_j \tau)^2 \right] \right\} \right\rangle_{r,\hat{\mathbf{x}}} . \tag{A.21}$$

Derivations with respect to q_0 and $\hat{q}_0$ give $2q_0\hat{q}_0 = C$ and functional derivatives with respect to $\pi(x)$ and $\hat{\pi}(\hat{x})$ give equations (15) of section 4.

Appendix A.2. MAC

In this case, $O = 1$,

$$\ln \Phi = \ln \frac{\left(2^L \hat{Q}_0\right)^C}{(C!)^L} + n \left\langle \ln \left\{ \sum_{\{\tau_i\}} \prod_{l=1}^{C} \prod_{i=1}^{L} \left(1 + \tau_i \hat{x}_i^l\right) \exp\left[- \frac{\beta}{2\sigma^2} \left(r - \sum_{i=1}^{L} S_i \tau_i \right)^2 \right] \right\} \right\rangle_{r,\hat{\mathbf{x}}} , \tag{A.22}$$

and the corresponding extremisation, including the necessary normalisation, gives equations (28) of section 5.

Appendix A.3. Interference Channel

The MIMO case with $L = O = 2$ can be viewed as an interference Gaussian channel where the receivers cooperate with each other to decode the received message. In this case

$$\Phi = \frac{\left(4\hat{Q}_0\right)^C}{C!} \left\langle \left\{ \sum_{\tau_1,\tau_2} \prod_{l=1}^{C} \left[\left(1 + \tau_1 \hat{x}_1^l\right)\left(1 + \tau_2 \hat{x}_2^l\right) \right] \times e^{-\frac{\beta}{2\sigma^2}(r_1 - S_{11}\tau_1 - S_{12}\tau_2)^2} e^{-\frac{\beta}{2\sigma^2}(r_2 - S_{21}\tau_1 - S_{22}\tau_2)^2} \right\}^n \right\rangle_{r,\hat{\mathbf{x}}} . \tag{A.23}$$

Extremisation with respect to π_i, $i = 1, 2$ results in

$$\hat{\pi}_i(\hat{x}_i) = \left\langle \delta\left(\hat{x}_i - \prod_{l=1}^{K-1} x_i^l \right) \right\rangle_{\mathbf{x}} , \tag{A.24}$$

and the functional derivative with respect to $\hat{\pi}_1$ gives

$$\frac{\delta \tilde{f}}{\delta \hat{\pi}_1(y_1)} = -nC\langle \ln\left(1+\hat{y}_1 x_1\right)\rangle_{\mathbf{x}}$$
$$+ nC\left\langle \ln\left[\sum_{\tau_1,\tau_2} P^{\tau_1\tau_2}(1+\tau_1\hat{y}_1)\prod_{l=1}^{C-1}\left(1+\tau_1\hat{x}_1^l\right)\prod_{l=1}^{C}\left(1+\tau_2\hat{x}_2^l\right)\right]\right\rangle_{r,\hat{\mathbf{x}}}, \quad \text{(A.25)}$$

where we defined

$$P^{\tau_1\tau_2} \equiv e^{-\frac{\beta}{2\sigma^2}(r_1-S_{11}\tau_1-S_{12}\tau_2)^2} e^{-\frac{\beta}{2\sigma^2}(r_2-S_{21}\tau_1-S_{22}\tau_2)^2}. \quad \text{(A.26)}$$

Equating to zero we obtain

$$\pi_1(x_1) = \langle \delta(x_1 - h_1(r,\hat{\mathbf{x}}))\rangle_{r,\hat{\mathbf{x}}}, \quad \text{(A.27)}$$

where

$$h_1(r,\hat{\mathbf{x}}) \equiv \frac{\sum_{\tau_1,\tau_2}\tau_1\, P^{\tau_1\tau_2}\prod_{l=1}^{C-1}\left(1+\tau_1\hat{x}_1^l\right)\prod_{l=1}^{C}\left(1+\tau_2\hat{x}_2^l\right)}{\sum_{\tau_1,\tau_2} P^{\tau_1\tau_2}\prod_{l=1}^{C-1}\left(1+\tau_1\hat{x}_1^l\right)\prod_{l=1}^{C}\left(1+\tau_2\hat{x}_2^l\right)}. \quad \text{(A.28)}$$

The final equations with the interference normalisation are already given in section 6 for both cases of a symmetric (subsection 6.1) and an asymmetric (subsection 6.2) interference channels. These equations can be easily generalised for any number of L and O values. In numerical calculations, however, the numerical errors occurring due to the introduction of additional fields in this direct form are difficult to control. Clever algebraic manipulations are necessary to keep these errors under control in order to obtain accurate results.